

# An ultrasonic motor for cryogenic temperature using bolt-clamped Langevin-type transducer

Daisuke Yamaguchi ,Takefumi Kanda, Koichi Suzumori

Graduate School of Natural Science and Technology, Okayama University, 3-1-1 Tsushima-naka,

Kita-ku, Okayama 700-8530, Japan

***Abstract :***

In this study, a small ultrasonic motor driven under cryogenic temperature conditions has been fabricated and evaluated.

Since transducer performance generally decreases at cryogenic temperatures, we designed and fabricated a bolt-clamped Langevin-type transducer for operation at cryogenic temperature. We simulated the influence of thermal stress on the transducer. The results from simulation were used to design the transducer, and it was then used to fabricate an ultrasonic motor for cryogenic temperature. The maximum diameter and the height of the motor are 30 mm and 38.7 mm.

To enable the motor to be driven at cryogenic temperature, we evaluated the relationship between the contact pre-load and the lowest rotatable temperature. The motor's driving performance was evaluated at both room temperature and cryogenic temperatures. In a 4.5 K helium gas ambient, the rotation speed and starting torque were 133 rpm and 0.03  $\mu$ Nm when the applied voltage was 50

$V_{p-p}$ .

Keywords: Ultrasonic motor; Cryogenic environment; Piezoelectric transducer; Actuator

## **1 Introduction**

Cryogenic environments provide important measuring conditions in advanced area of scientific research [1]–[3]. The temperature of cryogenic environments is near the liquid helium temperature, i.e., from under 20 to 4.2 K. In cryogenic environments, quantum-mechanical effects control various specific phenomena and these phenomena can be evaluated. Additionally, thermal noise in taking measurements is also very small in such environments [4].

Cryogenic temperature environments for measuring instruments are generally small in terms of space because otherwise it would be too difficult to maintain such environments. Nevertheless, there has been demand in recent years for actuators that can be rotated at high speed, over 1000rpm, under cryogenic temperature conditions [5].

Two major types of actuators are currently used at cryogenic temperature. The first has a driving source located outside the cryogenic environment [6]. It has high output power but the actuator system requires a great deal of space, which makes it difficult to maintain extreme environmental conditions. The second actuator is small and wholly located inside the cryogenic environment [7, 8]. It is used in the micro-positioning stage but its applications are limited.

To address these limitations, we have fabricated and evaluated a small ultrasonic motor that was driven under cryogenic temperature conditions. The motor's main feature was that it could rotate at higher speeds

than motors previously developed under these conditions. Ultrasonic motors can generally be easily downsized due to their driving principles [9]–[13]. Some of these have been used in several specific environments [14]–[16]. However, many current motors cannot be rotated under 77 K because their piezoelectric material characteristics at very low temperatures differ from those at room temperature. For example, the piezoelectric constant of PZT at cryogenic temperature is less than about a tenth of that at room temperature [17]. We therefore need a transducer that has high output to accomplish rotation under 77 K due to this decrease. The aim of our research was to achieve a transducer that had high output performance when the piezoelectric constant was decreased at cryogenic temperature.

We focused particularly on transducer performance and the motor's rotation in developing it. The output power of an ultrasonic motor is determined by using many parameters. We produced an ultrasonic motor in our previous research that could be rotated at 4.5 K by designing and assembling the transducer by taking into consideration the thermal compressive stress at ultralow temperature [18]. The performance of the motor generally increases by increasing the performance of the transducer. Therefore, we simulated thermal stress on the transducer, and fabricated and evaluated the transducer for operation at cryogenic temperature. An ultrasonic motor using the transducer, which took thermal stress into consideration was fabricated and evaluated after that.

The contact pre-load between the rotor and the transducer was adjusted for cryogenic temperature to enable the ultrasonic motor to be driven at cryogenic temperature. As a result, we have succeeded in rotating the motor at 4.5 K.

## **2 Structure of Motor and Underlying Driving Principles**

Figure 1 outlines the structure of the cryogenic ultrasonic motor. It is comprised of a bolt-clamped Langevin-type transducer, a rotor, some copper rings, a spring, a slit disk, two slide bearings, and two casings. The transducer is attached to the lower casing. The shaft joined to the rotor passes through the copper rings, the spring, and the bearings. The bearings are mounted inside the casing. The rotor is in contact with the transducer tip. The spring generates contact pre-load between the rotor and the transducer. The contact pre-load can be adjusted by varying the number of copper rings. The rotor is driven by traveling waves on the transducer tip and the friction force between the rotor and the transducer tip [19].

Velocity sensors, which are made of semiconductors, are generally not effective for the measuring rotation at cryogenic temperature. This is because semiconductor sensors have different characteristics at ultralow temperature from that at room temperature. For example, the resistance value at ultralow temperature becomes three times that at room temperature. Therefore, we fabricated an optical encoder to measure the rotation speed of the motor at such temperatures. The encoder, which was comprised a

reflective optical fiber sensor and a slit disk, is connected to the motor via a pair of optical fiber cables, one within the cryogenic temperature environment and one in a sensing station outside the environment.

Figure 2 shows photographs of the motor's parts and these of the assembled motor. The rotor and casings are made of stainless steel and the spring is made of titanium. The slide bearings are made of polytetrafluoroethylene (PTFE), which has a small frictional coefficient at cryogenic temperature. The stainless steel slit disk has 360 slits on its circumference.

The finite element method (FEM) was used to simulate the bearing's thermal shrinkage. The shrinkage was 47.4  $\mu\text{m}$  across the diameter when the temperature fell from 300 to 4.2 K. This shrinkage was taken into consideration in designing the gap between the rotor and the bearings.

The motor's maximum width and the height of the motor are 30 mm and 38.7 mm. The copper rings' weight is much less than the contact pre-load generated by the spring.

### **3 Bolt-Clamped Langevin-Type Transducer**

#### ***3.1 Design of Transducer***

In this study, we fabricated a bolt-clamped Langevin-type transducer. The piezoelectric performance of lead zirconate titanate ( $\text{Pb}(\text{Zr}_x\text{Ti}_{1-x})\text{O}_3$ , PZT) is very poor at cryogenic temperature. A transducer for an

ultrasonic motor and a piezoelectric actuator is generally achieved by using various structures, for example some laminated piezoelectric transducers. An organic bond is used for such transducers to paste both component materials. These organic materials are damaged at cryogenic temperature and the transducers break down. However, a bolt-clamped Langevin-type transducer consists of various ceramics and some metal materials. Bolt-clamped Langevin-type transducers can be used in cryogenic temperature environments because of this. In addition, the transducers also perform well with high levels of vibration because the Q value is large. These advantages enable the transducers to be used at cryogenic temperature.

There is schematic of a transducer in Fig. 3. It consists of a body, a bolt, a nut, two ring electrodes, four quartered electrodes, and two PZT rings. The PZT rings are 0.2 mm thick and are polarized in the thickness direction. The bolt passes through the ring electrodes, PZT rings, and the quartered electrodes. The nut is tightly clamped down onto the body and a generated pre-load is applied to the transducer. A sinusoidal voltage with a 90 deg phase difference is applied to each quartered electrode. The transducer therefore generates two flexural vibration modes perpendicularly, and traveling waves are generated on the transducer's tip. This kind of operating principle is called a "mode rotational type" [20].

The transducer was designed by using commercial package FEM software, ANSYS. The model of this analysis is shown in Fig. 4, and the results obtained from modal analysis are given in Fig. 5. The model was meshed by hexahedral element. The mounted area of the flange in this analysis was constrained in

omni-directionally, which was the same as the conditions in use. The transducer was designed to have a node at the flange. An anti-node of the bending vibration generally has maximum bending stress and high output power. Our transducer, on the other hand, is affected by a thermal compressive stress when the temperature is decreased from room temperature to cryogenic temperature. If the transducer has the piezoelectric material at the anti-node of bending vibration, the material will be damaged by these stresses when the temperature decreased. There are piezoelectric materials at node because of this.

### ***3.2 Thermal influence on transducer***

As mentioned in Section 3.1, a bolt-clamped Langevin-type transducer has a number of advantages that can be used at cryogenic temperature. However, its pre-load is affected by thermal stress generated when room temperature falls to cryogenic temperature. Since this stress damages the transducer's piezoelectric materials, we used FEM thermal-structural analysis to estimate it. In this simulation, we used all the material's coefficients of thermal expansion (CTE) and Young's moduli of metal materials as non-linear material properties with temperature [21]–[24]. The PZT stiffness and Poisson ratio of all materials were used for the value of room temperature because the change in characteristics was small at cryogenic temperature [24]. An example of the material properties used in the simulation is shown in Fig. 6 [23]. The contact between the two elements that have different materials was modeled as a node shared by

these elements.

Figure 7(a) shows an expanded view of the results obtained from simulation when the temperature was lowered from 300 to 60 K. The cross-sectional view at the piezoelectric material is shown in Fig 7(b). The maximum thermal stress on the PZT rings was 73.0 MPa of compressive stress when the transducer's temperature fell from 300 to 60 K. The transducer was designed and assembled to prevent the total stress of the transducer from exceeding a failure stress.

### ***3.3 Fabrication of transducer***

Figure 8 has photographs of the fabricated transducer. Its diameter, height, and flange diameter corresponded to 6, 16 and 20 mm, respectively. The quartered electrode was cut into quarters after being assembled.

The clamping torque was estimated to be 0.7 Nm from the result of thermal-structural analysis and the relationship between clamping torque and transducer's admittance [18].

### ***3.4 Evaluation of transducer***

The measured distribution for the transducer's vibration velocity is plotted in Fig. 9. The transducer in

this experiment was supported at its flange. We used a laser Doppler vibrometer to measure the transducer's vibration velocity. The applied voltage and driving frequency were  $25 V_{p-p}$  and 76.10 kHz. The fabricated transducer had a nodal position at the flange and at the piezoelectric material. The transducer generated the same vibration mode under these conditions as that obtained from the simulation results.

Figure 10 plots the relationship between vibration velocity and driving frequency. The maximum velocity was 236 mm/s when the applied voltage and the driving frequency were  $50 V_{p-p}$  and 76.10 kHz.

#### **4 Driving Performance at Room temperature**

We evaluated the relationship between the rotor's contact pre-load applied to the transducer and the rotation speed at room temperature. We measured the rotation speed with a laser surface velocimeter. The contact pre-load is increased due to decreasing the temperature because the elastic coefficient of the material using a spring is increased. The contact pre-load value was determined from the pre-load when the motor was rotated at its lowest temperature, i.e., 0.139 N, from this reason. The value of the contact pre-load was calculated by using spring constant and distance between the bearing and the copper rings. The contact pre-load was changed by varying the number of copper rings between the spring and the rotor.

Figure 11 plots the relationship between the contact pre-load and the rotation speed at room temperature when the applied voltage was 50 V<sub>p-p</sub>. The maximum rotation speed was 695.6 rpm when the contact pre-load and driving frequency were 0.168 N and 75.84 kHz. When the contact pre-load was 0.139 N, the motor did not have continuous rotation

We calculated the starting torque from the transient response of the motor at room temperature. Starting torque  $T_0$  can be estimated by

$$T_0 = \frac{\Omega_0 J}{\tau}, \quad (1)$$

where  $\Omega_0$ ,  $J$ , and  $\tau$  correspond to the saturated revolution speed, the inertia of the rotor, and the time constant [25].

The time constant was  $9.77 \times 10^{-3}$  s when the applied voltage, electrical current, and contact pre-load were 50 V<sub>p-p</sub>, 20.8 mA<sub>p-p</sub>, and 0.168 N. The starting torque was calculated to be 9.1  $\mu$ Nm under these conditions. The torque was small because the motor was designed to be able to be rotated at cryogenic temperature.

## 5 Cryogenic Actuator Evaluation System

In this study, we used a cryogenic actuator evaluation system to measure the fabricated motor's specifications at cryogenic temperature. There is a schematic of the system in Fig. 12, which consists of

an insert system and a liquid helium tank.

The insert system, which is rod-like in shape and inserted into the liquid helium tank, has 10 electronic terminals and one pair of optical terminals. A sample (e.g., motor) is mounted on the tip of the insert system. Figure 13 shows our motor mounted on it. The tip of the insert system has a heater and a temperature sensor; we used the latter to measure the temperature in our experiments. The cryogenic temperature was obtained by using helium gas in the liquid helium tank. The more the helium gas temperature is lowered, the closer to a liquid helium state it becomes. The motor's temperature is controlled by the insert system's position and fine tuned by using the heater.

## **6 Driving Performance at Cryogenic Temperature**

We measured the ultrasonic motor's driving performance at cryogenic temperature. The temperature was obtained with the cryogenic actuator evaluation system shown in Fig. 12. The rotation speed in this study was measured with the fabricated optical encoder shown in Fig. 1.

Since Young's modulus increases at low temperature and has non-linear characteristics at cryogenic temperature, the motor's spring constant increases. The shrinkage ration of the spring and casing is much smaller than the increasing ratio the spring constant. The contact pre-load increases at cryogenic temperature. We evaluated the relationship between the rotation performance and the contact pre-load in

this study. The contact pre-load was adjusted by varying the number of copper rings. The ring's thermal shrinkage was found to influence driving performance much less than the increased spring constant.

Figure 14 plots the relationship between the motor's contact pre-load to the transducer and the lowest rotatable temperature when the applied voltage was  $50V_{p-p}$ . The lowest rotatable temperature was defined as the temperature at which the motor could rotate continuously. The contact pre-load value was that adjusted for room temperature. The resonance frequency of the transducer differed at each temperature because the Young's moduli of all materials increase as the temperature falls. Therefore, we adjusted the driving frequency at each temperature.

The lowest rotatable temperature under these conditions was found to depend on the contact pre-load. The contact pre-load value at which the motor can be rotated has narrow range at cryogenic temperature because the performance of the transducer degrades at cryogenic temperature. In addition, the contact pre-load value at cryogenic temperature is larger than that at room temperature because the spring constant is increased due to decreasing temperature. Therefore, it was necessary to adjust the contact pre-load for cryogenic temperature.

Figure 15 plots the relationship between the temperature, the rotation speed, and the starting torque. The starting torque was calculated with Eq. (1). The contact pre-load and applied voltage were 0.139 N and  $50V_{p-p}$ , respectively. The rotation speed and starting torque were 131 rpm and  $0.03 \mu\text{Nm}$  at 4.5 K when the electrical current was  $21 \text{ mA}_{p-p}$ . When the temperature fell, the rotation speed and starting torque initially

decreased. The rotation speed remained constant under 60 K.

Figures 16 (a) and (b) shows the relationship between frequency, admittance of the transducer, and phase when the transducer's temperature was 290 K and 4.5 K, respectively. The resonant frequency increased at ultralow temperature because the elastic coefficient of the material use the transducer increased. The admittance at 4.5 K was lower than that at 290 K. Figure 17 plots the relationship between the temperature and, admittance of the transducer. The admittance initially decreased when the temperature was lowered but remained at a constant value under 90 K.

Good similarities can be found by comparing Figs. 15 and 17. These similarities indicate that the decreases in rotation speed and starting torque are mainly attributable to degradation in the transducer's performance.

## **7 Conclusions**

A cryogenic ultrasonic motor designed to operate at cryogenic temperature was fabricated and evaluated in this study. The motor's primary component was a bolt-clamped Langevin-type transducer for cryogenic temperature. To produce the transducer, we simulated its thermal stress with thermal structural analysis. The maximum thermal stress was found to be 73.0 MPa when the temperature fell from 300 to 60 K. We used this in designing and assembling the transducer.

We evaluated driving performance of the motor by evaluating the contact pre-load between the rotor and

the transducer. The maximum rotation speed and starting torque were 695.6 rpm and 9.1  $\mu\text{Nm}$  at room temperature when the applied voltage and contact pre-load were 50  $V_{\text{p-p}}$  and 0.168 N.

We evaluated the relationship between the contact pre-load and the lowest rotatable temperature to achieve a motor that could be operated at cryogenic temperature. The results obtained were used in adjusting the contact pre-load for cryogenic temperature.

We have succeeded in driving the motor at cryogenic temperature. The rotation speed and starting torque were 133 rpm and 0.03  $\mu\text{Nm}$  at 4.5 K when the applied voltage and the contact pre-load were 50  $V_{\text{p-p}}$  and 0.139 N.

## Acknowledgements

This work was partially supported by the Grants-in-Aid for Young Scientists (B) (No. 21760114) of the Ministry of Education, Culture, Sports, Science and Technology, Japan.

## References

- [1] Y. Fujiyoshi, T. Mizusaki, K. Morikawa, H. Yamagishi, Y. Aoki, H. Kihara, and Y. Harada, "Development of a superfluid helium stage for high-resolution electron microscopy", *Ultramicroscopy*, Vol. 38, 1991, pp. 241–251.
- [2] K. Saitoh, K. Hayashi, Y. Shibayama, and K. Shirahama, "A low temperature scanning probe microscope using a quartz tuning fork", *International Conference on Low Temperature Physics*, 150, 2009, 012039.
- [3] N. Suehira, Y. Tomiyoshi, K. Sugiyama, S. Watanabe, T. Fujii, Y. Sugawara, and S. Morita "Development of low temperature ultrahigh vacuum non contact atomic force microscope with PZT cantilever", *Applied Surface Science*, 157, 2000, pp. 343–348.
- [4] T. Mizuno, K. Hioka, K. Fujioka and K. Takegoshi, "Development of magic-angle spinning nuclear magnetic resonance probe with a cryogenic detection system for sensitivity enhancement", *Review of Scientific Instruments*, 79, 2008, 044706.

- [5] M. Kubota, T. Obata, R. Ishiguro, M. Yamashita, T. Igarashi, E. Hayata, O. Ishikawa, Y. Sasaki, N. Mikhin, M. Fukuda, V. Kovacik, Y. Sasaki, N. Mikhin, M. Fukuda, V. Kovacik, and T. Mizusaki, "Superfluidity and quantized vortex studies under rotation up to 4 Hz at mK and 1Hz sub-mK temperatures", *Physica B* 329–333, 2003, pp. 1577–1581.
- [6] R. Shively, "Submerged cryogenic motor materials development", *IEEE Electrical Insulation Magazine*, Vol. 19, No. 3, 2003, pp. 7–11.
- [7] S. Dong, L. Yan, N. Wang, and D. Viehland, "A small, linear, piezoelectric ultrasonic cryomotor", *Applied Physics Letters*, 86, 2005.
- [8] S. Dong, L. Yan, D. Viehland, X. Jiang, and W. S. Hackenberger, "A piezoelectric single crystal traveling wave step motor for low-temperature application", *Applied Physics Letters*, 92, 2008.
- [9] T. Kanda, A. Makino, T. Ono, K. Suzumori, T. Morita, and M. K. Kurosawa, "A micro ultrasonic motor using a micro-machined cylindrical bulk PZT transducer", *Sensors and Actuators A*, 127, 2006, pp. 131–138.
- [10] T. Kanda, T. Ichihara, and K. Suzumori, "Design and evaluation of low-profile micro ultrasonic motors driven by sector shaped piezoelectric vibrators", *2009 IEEE International Ultrasonics Symposium Proceedings*, 2009, pp.2596–2599.
- [11] T. Ichihara, T. Kanda, and K. Suzumori, "Design and evaluation of low-profile micro ultrasonic motors using sector shaped piezoelectric vibrators", *2008 IEEE International Conference on Intelligent Robots and Systems*, 2008, pp.588–593.
- [12] T. Morita, "Miniature piezoelectric motor", *Sensors and Actuators*, 2003, 103–3, pp.291–300.
- [13] M. Aoyagi, Y. Tomikawa, and T. Takano, "Ultrasonic Motors Using Longitudinal and Bending Multimode Vibrators with Mode Coupling by Externally Additional Asymmetry or Internal Nonlinearity", *Japanese Journal of Applied Physics*, 31, 1992, pp.3077–3080.
- [14] T. Morita, T. Niino and H. Asama "Rotational feedthrough using a ultrasonic motor for ultra-high vacuum conditions", *Vacuum*, 2002, 65, pp.85–90.
- [15] T. Morita, S. Takahashi, H. Asama, and T. Niino, "Rotational feedthrough using an ultrasonic motor and its performance in ultra high vacuum conditions", *Vacuum*, 70, 2003, pp.53–57.
- [16] H. Maeda, A. Kobayashi, T. Kanda, and K. Suzumori, "A cylindrical ultrasonic motor for NMR sample spinning in high magnetic field", *2009 IEEE International Ultrasonics Symposium Proceedings*, 2009, pp.1070–1073.
- [17] D. Grupp, and A. Goldman, "Giant piezoelectric effect in strontium titanate at cryogenic temperatures", *Science*, 276, 1997, pp. 392–394.
- [18] D. Yamaguchi, T. Kanda, and K. Suzumori, "Bolt-clamped Langevin-type transducer for ultrasonic motor used at ultralow temperature", *Journal of Advanced Mechanical Design, Systems, and Manufacturing*, 6, No. 1, 2012, pp. 104–112.
- [19] M. Kurosawa, K. Nakamura, T. Okamoto, and S. Ueha, "An ultrasonic motor using bending vibrations of a short cylinder", *IEEE Transactions on Ultrasonics, Ferroelectrics, and Frequency control*, 36, No. 5, 1989, pp. 517–521.
- [20] T. Morita, M. Kurosawa, and T. Higuchi, "An ultrasonic micromotor using a bending cylindrical transducer based on PZT thin film", *Sensors and Actuators A*, 50, 1995, pp. 75–80.
- [21] Y. Takeuchi, N. Noda, S. Komori, and T. Yamamoto, "Temperature dependence of elastic moduli of several steels at low temperature range", *The Society of Materials Science*, 28, pp. 852–856, (in Japanese).
- [22] H. M. Ledbetter, "Temperature behaviour of Young's moduli of forty engineering alloys", *Cryogenics*, 1982, pp. 653–656.

- [23]R. H. Bogaard, P. D. Desai, H. H. Li, and C. Y. Ho, "Thermophysical properties of stainless steels", *Thermochimica Acta*, 218, 1993, pp. 373–393.
- [24]R. P. Taylor, G. F. Nellis, S. A. Klein, D. W. Hoch, J. Fellers, P. Roach, J. M. Park, and Y. Gianchandani, "Measurements of the material properties of a laminated piezoelectric stack at cryogenic temperatures", *Advances in Cryogenic Engineering: Transactions of the International Cryogenic Materials Conference*, 52, 2006, pp. 200–207.
- [25]K. Nakamura, M. Kurosawa, H. Kurebayashi, and S. Ueha, "An Estimation of Load Characteristics of an Ultrasonic Motor by Measuring Transient Responses", *IEEE Transactions on Ultrasonics*, 38, No. 5, 1991, pp. 481–485.

## Biographies

Daisuke Yamaguchi was born on May 1, 1986. He received his B. Eng. and M. Eng. from Okayama University, in Japan in 2009 and 2011. Since then, he has been a doctoral student at the same university. His current research interests are in piezoelectric actuators and mechatronics.

He is a member of the Japan Society of Mechanical Engineers, the Robotics Society of Japan, and the Japan Society for Precision Engineering.

Takefumi Kanda was born in Fukuoka, Japan, on June 18, 1972. He received his B. Eng., M. Eng. and Dr. Eng. in precision machinery engineering from the University of Tokyo, in 1997, 1999, and 2002.

From 2002 to 2007, he was a research associate and lecturer at Okayama University in Japan. Since 2007, he has been an associate professor at the same university. His research interests are in micro sensors, micro actuators, micro systems, and piezoelectric film.

He is a member of the Japan Society for Precision Engineering, the Institute of Electrical Engineers of Japan, IEEE, the Japan Society of Mechanical Engineers, and the Robotics Society of Japan.

Koichi Suzumori was born in 1959. He received his doctorate from Yokohama National University in 1990. He worked for the Toshiba R&D Center from 1984 to 2001 and for the Micromachine Center, Tokyo, from 1999 to 2001. He has been a professor at Okayama University, Japan since 2001.

He is a member of the Japan Society of Mechanical Engineers, the Robotics Society of Japan, IEEE and the Institute of Electrical Engineers of Japan.

Fig. 1 Structure of ultrasonic motor for cryogenic temperature

Fig. 2 Fabricated ultrasonic motor for cryogenic temperature; (a) Component parts, and (b)

Assembled motor

Fig. 3 Structure of bolt-clamped Langevin-type transducer

Fig. 4 Model of FEM modal analysis for transducer meshed by hexahedral element

Fig. 5 Results of FEM modal analysis for transducer

Fig. 6 Example of non-linear material's properties with temperature and coefficient of thermal expansion (CTE) of SUS304

Fig. 7 Thermal structural analysis result for temperature drop from 300 K to 60 K; (a) overall view, and (b) cross-sectional view

Fig. 8 Bolt-clamped Langevin-type transducer for cryogenic environment; (a) Component parts of transducer, and (b) Fabricated transducer

Fig. 9 Vibration velocity distribution for transducer

Fig. 10 Relationship between vibration velocity and driving frequency at room temperature

Fig. 11 Relationship between contact pre-load and rotation speed at room temperature

Fig. 12 Photograph and cross sectional view of cryogenic actuator evaluation system

Fig. 13 Expanded view around tip of insert system

Fig. 14 Relationship between contact pre-load and lowest rotatable temperature

Fig. 15 Relationship between temperature, rotation speed, and starting torque

Fig. 16 Relationship between frequency, admittance of transducer, and phase; (a) At 290K, and (b)

At 4.5 K

Fig. 17 Relationship between temperature and admittance of transducer

Fig.1

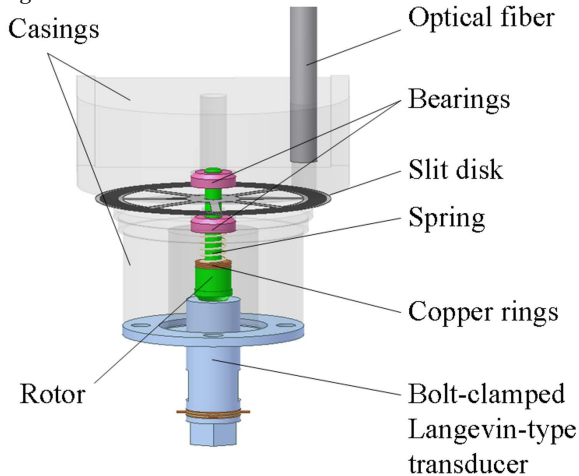


Fig.2(a)

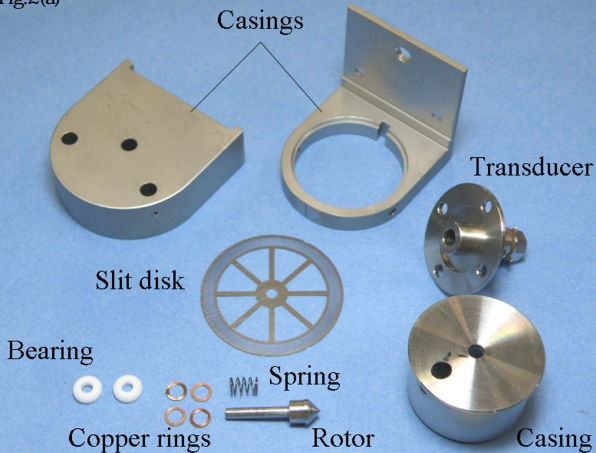
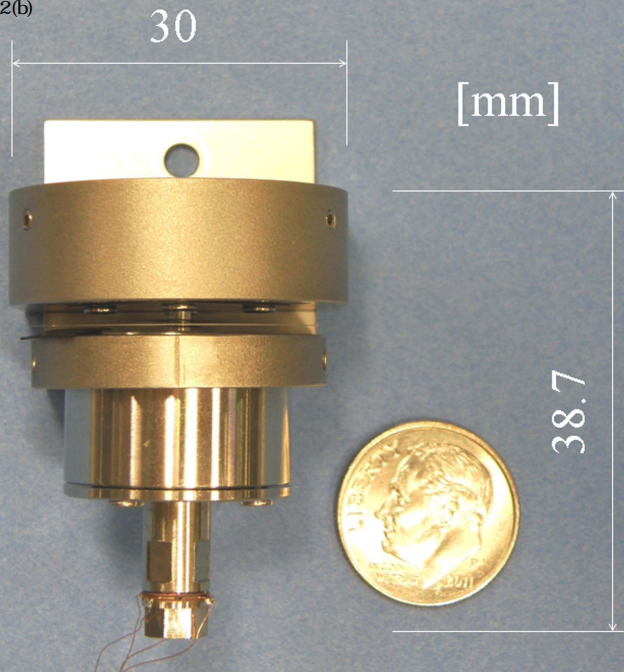
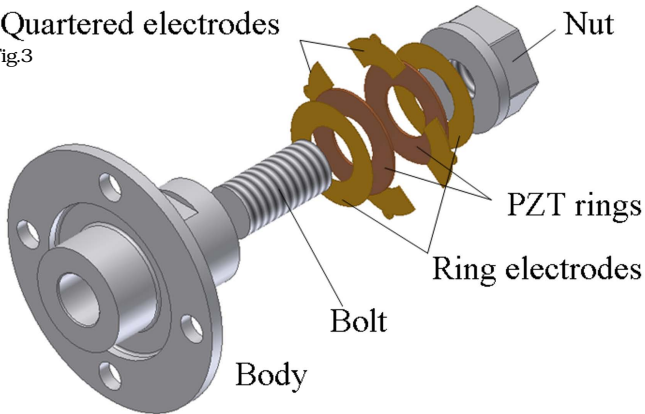


Fig.2(b)



# Quartered electrodes

Fig.3

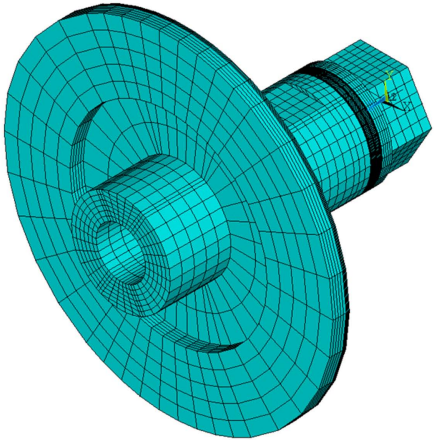


1

ELEMENTS

Fig.4

OCT 6 2010  
17:30:22  
PLOT NO. 1



1

NODAL SOLUTION

STEP=1  
SUB =9  
FREQ=82516  
USUM (AVG)  
RSYS=0  
DMX =41.106  
SMN =.249244  
SMX =41.106

Fig.5



SEP 29 2010  
11:04:02  
PLOT NO. 1

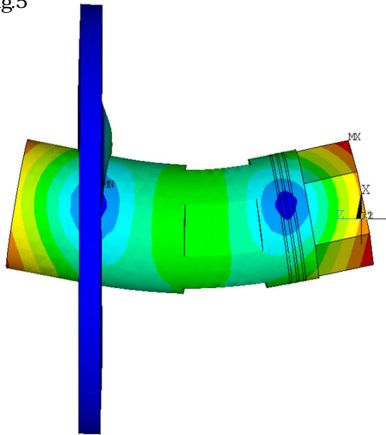
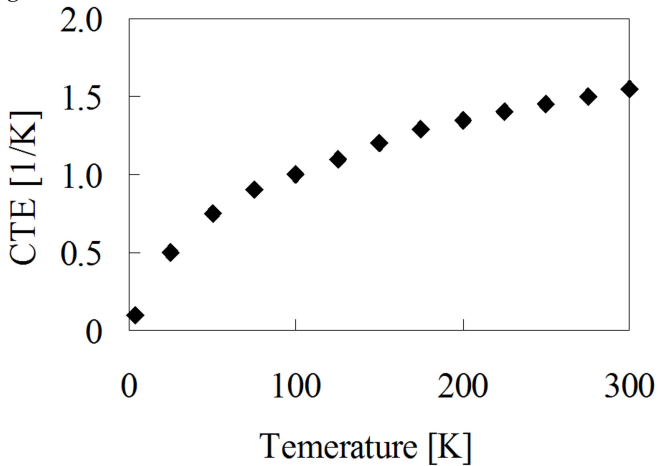


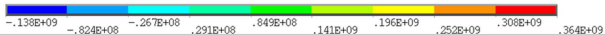
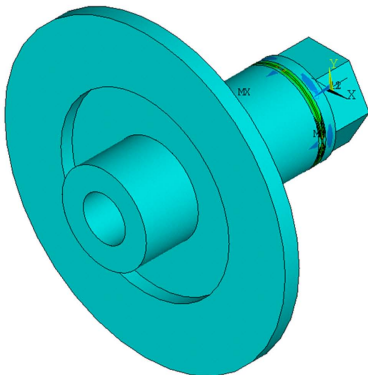
Fig.6



1

NODAL SOLUTION

Fig.7(a)

APR 21 2012  
16:05:48  
PLOT NO. 1STEP=1  
SUB =1  
TIME=1  
SZ (AVG)  
RSYS=0  
DMX =.505E-04  
SMN =-.138E+09  
SMX =.364E+09

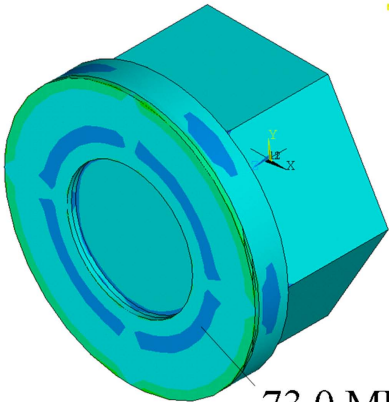
1

Fig.7(b)

APR 21 2012  
16:21:09  
PLOT NO. 1

NODAL SOLUTION

SUB =1  
TIME=1  
SZ (AVG)  
RSYS=0  
DMX =.505E-04  
SMN =-.138E+09  
SMX =.364E+09



73.0 MPa

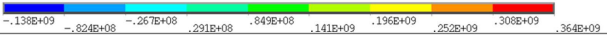


Fig.8(a)



Body

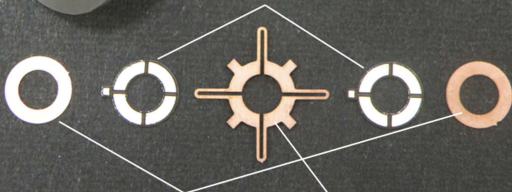
Bolt



Nut



PZT rings



Ring electrodes

Quartering electrodes

Fig.8(b)



Fig.9

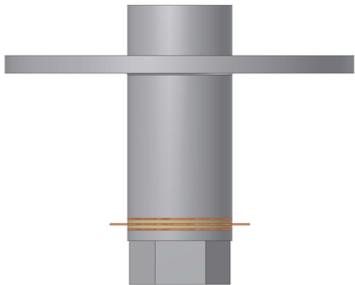
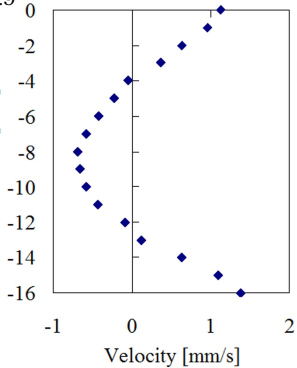


Fig.10

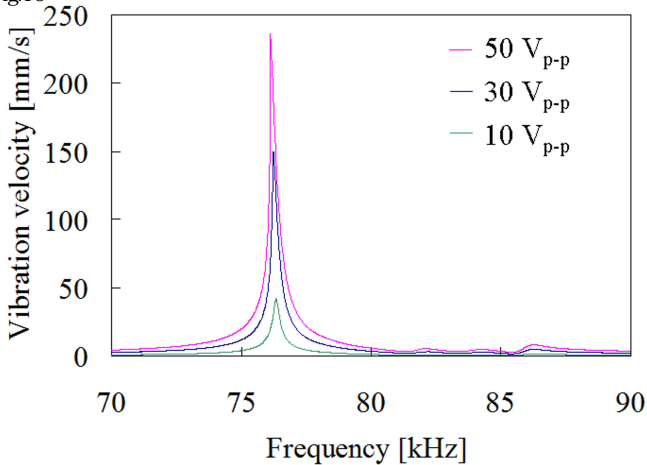


Fig11

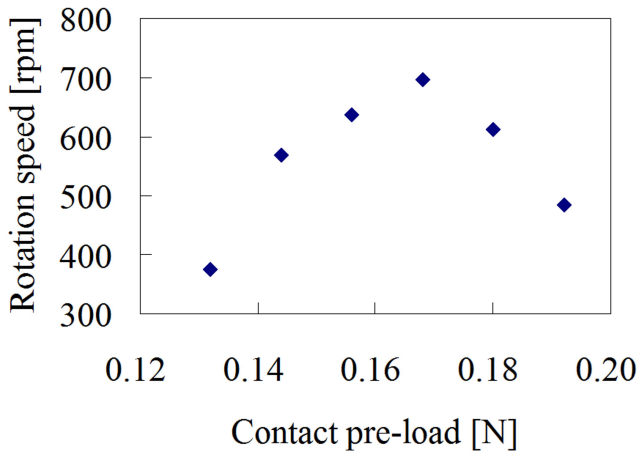


Fig.12

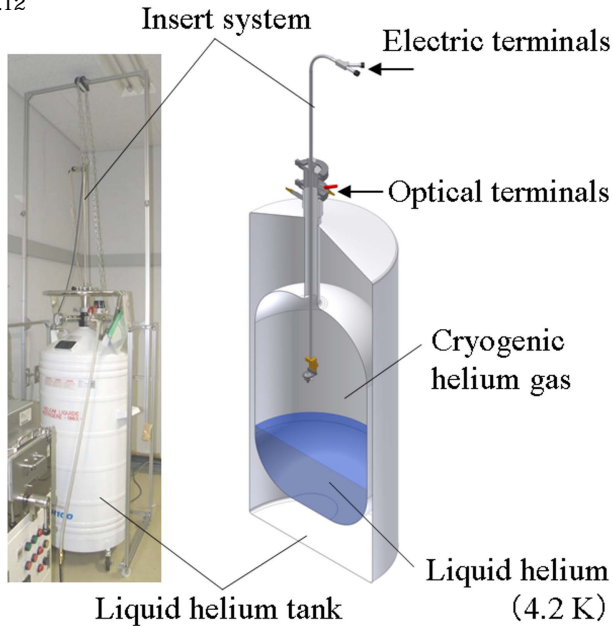


Fig.13

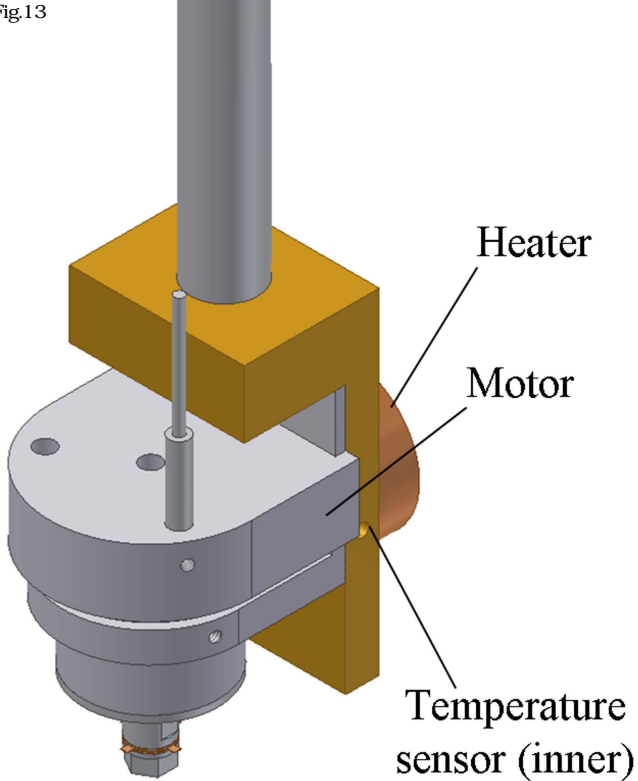


Fig.14

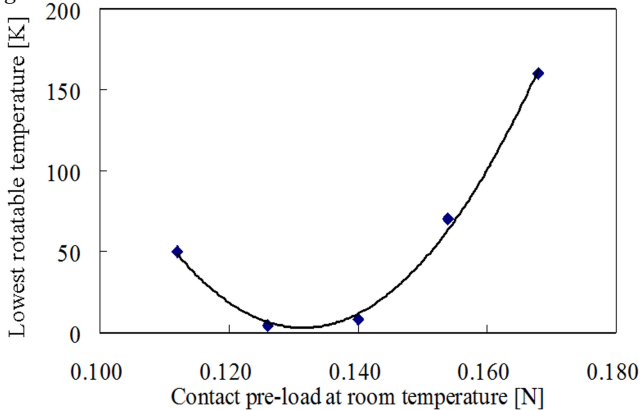


Fig.15

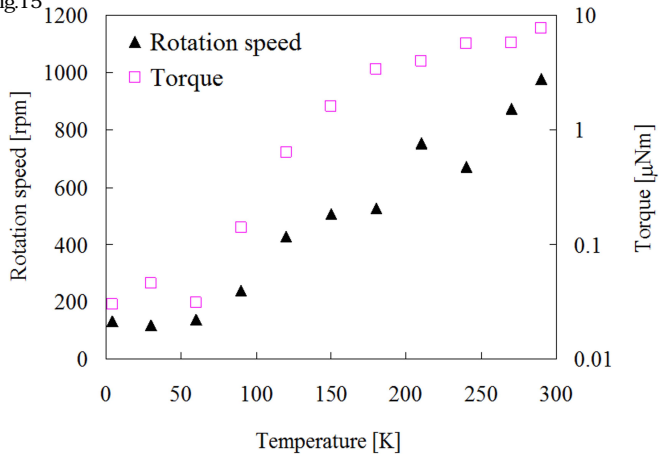


Fig.16(a)

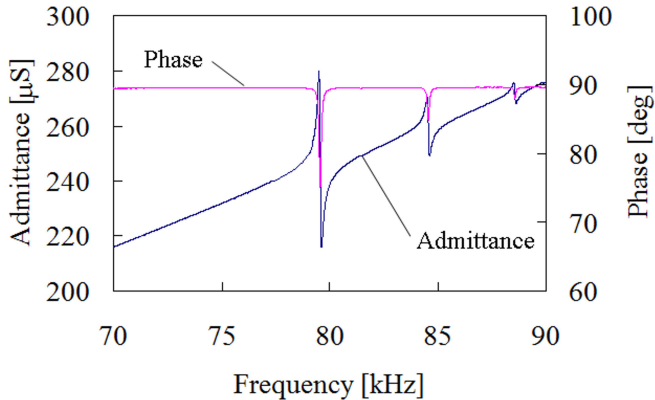


Fig.16(b)

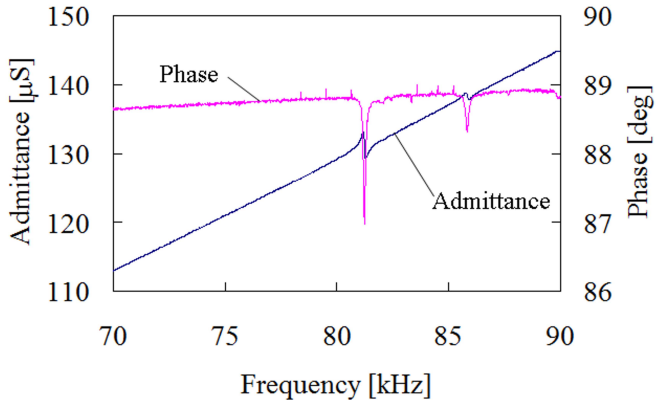


Fig.17

